Inorganic Chemistry

ARTICLE

pubs.acs.org/IC

Pore with Gate: Enhancement of the Isosteric Heat of Adsorption of Dihydrogen via Postsynthetic Cation Exchange in Metal−Organic Frameworks

Sihai Yang,[†] Gregory S. B. Martin,[†] Jeremy J. Titman,[†] Alexander J. Blake,[†] David R. Allan,[‡] Neil R. Champness,*[,†] and Martin Schröder*[,†]

[†]School of Chemistry, University of Nottingham, University Park, Nottingham NG7 2RD, U.K.

[‡]Diamond Light Source, Harwell Science and Innovation Campus, Didcot, Oxfordshire OX11 0DE, U.K.

Supporting Information

ABSTRACT: Three isostructural anionic frameworks $\{[(Hdma)(H_3O)][In_2(L^1)_2]\cdot 4DMF\cdot 5H_2O\}_\infty$ (NOTT-206-solv), $\{[H_2ppz][In_2(L^2)_2]\cdot 3.5DMF\cdot 5H_2O\}_\infty$ (NOTT-200-solv), and $\{[H_2ppz][In_2(L^3)_2]\cdot 4DMF\cdot 5.5H_2O\}_\infty$ (NOTT-208-solv) (dma = dimethylamine; ppz = piperazine) each featuring organic countercations that selectively block the channels and act as pore gates have been prepared. The organic cations within the as-synthesized frameworks can be replaced by Li^+ ions to yield the corresponding Li^+-containing frameworks $\{Li_{1.2}(H_3O)_{0.8}[In_2(L^1)_2]\cdot 14H_2O\}_\infty$ (NOTT-207-solv), $\{Li_{1.5}(H_3O)_{0.5}[In_2(L^2)_2]\cdot 11H_2O\}_\infty$ (NOTT-201-solv), and $\{Li_{1.4}(H_3O)_{0.6}[In_2(L^3)_2]\cdot 4acetone\cdot 11H_2O\}_\infty$ (NOTT-209-solv) in which the pores are now unblocked. The desolvated framework materials NOTT-200a, NOTT-206a, and NOTT-208a display nonporous, hysteretic and reversible N_2 uptakes, respectively, while NOTT-206a and NOTT-200a provide a strong kinetic trap showing adsorption/desorption hysteresis with H_2. Single crystal X-ray analysis confirms that the Li^+ ions are either tetrahedrally (in NOTT-201-solv and NOTT-209-solv) or octahedrally (in NOTT-207-solv) coordinated by carboxylate oxygen atoms and/or water molecules. This is supported by ^7Li solid-state NMR spectroscopy. NOTT-209a, compared with NOTT-208a, shows a 31% enhancement in H_2 storage capacity coupled to a 38% increase in the isosteric heat of adsorption to 12 kJ/mol at zero coverage. Thus, by modulating the pore environment via postsynthetic cation exchange, the gas adsorption properties of the resultant MOF can be fine-tuned. This affords a methodology for the development of high capacity storage materials that may operate at more ambient temperatures.

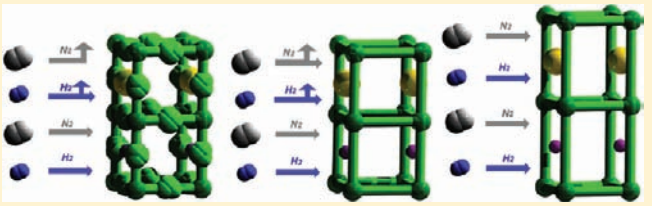

INTRODUCTION

Charged porous framework materials have not been widely studied for gas storage applications,[1−11] with the vast majority of studies focusing on neutral systems.[12−20] This is a logical stance given that a charged framework must by definition incorporate counterions within the pore channels, which will inevitably reduce the effective porosity and may block some pores completely.[21−23] Attempts to remove or extract the counterions and/or organic template from the as-synthesized network solid often lead to decomposition and amorphization of the framework with loss of microporosity.[24−27] We describe herein new anionic framework materials in which the choice of associated cation can modulate and enhance their properties and function. By postsynthetic cation exchange it is possible to generate different materials derived from the same parent framework structure: these incorporate different cations which may, by appropriate design, be located at the pore entrance and act as a "pore gate", leading to a variety of functionalities in these materials.

Metal−organic framework (MOF) materials are effective stores for hydrogen (H_2), but a major limitation is that they only show significant storage capacities at cryogenic temperatures (typically 77 K), reflecting the low binding energy of physisorption. Recent computational and theoretical studies on the modeling of H_2 adsorbed into Li-doped MOF hosts suggest this to be an effective mechanism for increasing H_2 binding energies and thereby increasing the storage temperatures at which these materials operate.[28−34] However, doping of active Li(0) into a real MOF material is problematic experimentally due to the high reactivity of Li(0) toward the cationic metal clusters and organic ligands that constitute these porous structures. Hupp et al. have reported Li-doping (∼5 mol % Li) of a MOF via chemical reaction with Li metal and confirmed increases in both the isosteric heat and the overall H_2 adsorption uptake.[35−37] However, this enhancement has been attributed to displacement of frameworks within the interpenetrated structure during the intense chemical reduction and incorporation of Li(0), rather than to any direct Li−H_2 interactions. Eddaoudi et al. have also reported enhanced isosteric heat of adsorption for H_2 in a Li^+-exchanged Li-*rho*-ZMOF material.[6,38] However, the Li^+ centers

Received: May 9, 2011
Published: September 07, 2011

Scheme 1. Charged NOTT-MOF Materials Incorporating Different Countercations and Cation-Exchange Processes[a]

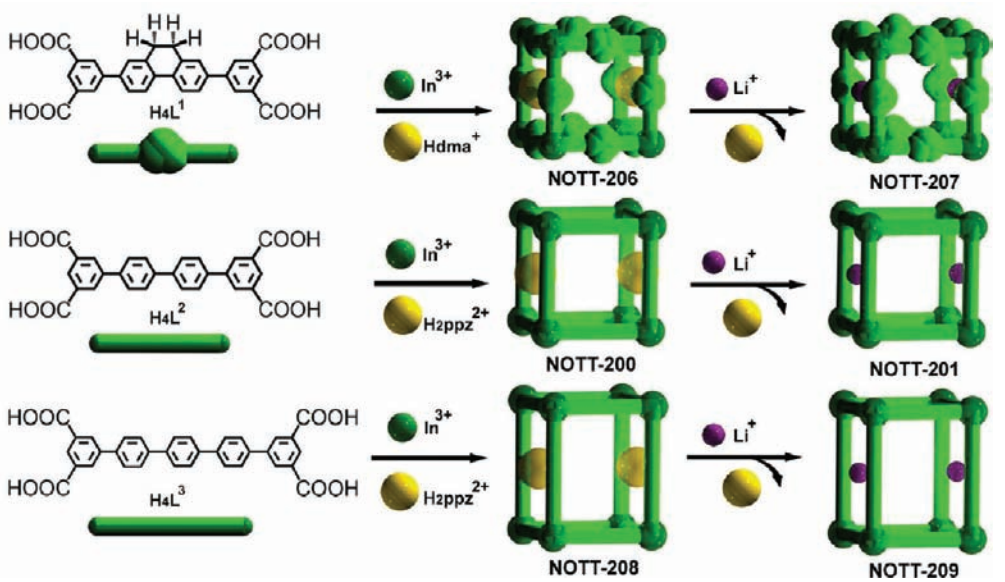

[a] Both NOTT-200 and NOTT-208 contain H_2ppz^{2+} countercations; NOTT-206 contains $Hdma^+$ cations. The doubly interpenetrated $(3\text{-c})_2(4\text{-c})$ ***tfa*** nets in these materials have been simplified to non-interpenetrated 6-c ***pcu*** cages for purposes of clarity.

are highly disordered within the framework, and their locations have not been determined, making it impossible to establish the geometry of any potential coordination at the Li^+ center. In the corresponding desolvated material the Li^+ cations remain fully coordinated to four water molecules, the removal of which at 300 °C leads to collapse of the framework. The Li^+ centers are, therefore, not accessible to H_2 molecules, and any enhancement in the heat of adsorption has been attributed to the electrostatic field from the charged framework and counterions. An isosteric heat of adsorption of ~15−20 kJ mol^{-1} is required for a H_2 storage system operating closer to ambient temperature and at pressures below 20 bar for delivery to a H_2 fuel cell.[39] H_2 adsorption in most MOF materials gives an average adsorption enthalpy of 4−7 kJ mol^{-1},[12−20] and methodologies aimed at increasing binding within pores are, therefore, of major interest.

Our approach is based upon the linking of tetrahedral nodes derived from In(III) centers bound to bis-isophthalate tetracarboxylates to form 4-connected (4-c) 3-D network structures. The discrepancy between the charge on In(III) and the negative organic linker L^{4-} leads to the formation of anionic complexes $[In(L)]^-$ in which the net charge has to be balanced by a countercation. Varying the length or functionality of the organic ligand allows fine-tuning of the pore environments, which can incorporate different cationic guest molecules. Furthermore, the countercations within the as-synthesized materials are exchangeable while still maintaining the porosity of the framework structure. In this way, pores can be simultaneously decorated by functionality from both the polyaromatic organic linkers bound to In(III) via carboxylates, and from the countercations located within the pore. This endows the pores with a new level of complexity and functionality exceeding that of simple neutral MOF materials.

EXPERIMENTAL SECTION

All chemical reagents and gases were obtained from commercial sources and, unless otherwise noted, were used without further purification.

Ligand Synthesis. Ligands H_4L^1, H_4L^2, and H_4L^3 were synthesized using the previously reported method.[20]

Preparation and Characterization of Metal Complexes. All materials were obtained in microcrystalline form and good phase purity via the experimental procedure as described below. The original framework materials were synthesized by solvothermal reactions of organic ligands and $In(NO_3)_3$. To establish the influence of the cationic species on the pore environment and gas storage properties, H_2ppz^{2+} or $Hdma^+$ cations in the original framework materials were replaced by Li^+ cations via ion-exchange under mild conditions (Scheme 1). The composition of these complexes was confirmed by single crystal X-ray diffraction, elemental and inductively coupled plasma mass spectrometry (ICP-MS) analysis, infrared spectroscopy (IR), and thermogravimetric analysis (TGA). The purity of the bulk materials was confirmed by powder X-ray diffraction (PXRD) and elemental analysis. Samples were solvent-exchanged with acetone, which was repeated 10 times over 4 days, and the solvent-exchanged samples were kept in acetone. For gas adsorption and solid-state NMR experiments, the acetone-exchanged material was desolvated at 100−120 °C under dynamic vacuum to afford desolvated porous materials. PXRD of bulk samples of NOTT-200-solv, NOTT-201-solv, NOTT-206-solv, NOTT-207-solv, NOTT-208-solv, and NOTT-209-solv are consistent with the single crystal X-ray data for each, and confirm that the framework structure remains intact after Li^+-exchange (see Supporting Information).

The syntheses of $\{[H_2ppz][In_2(L^2)_2]\cdot 3.5DMF\cdot 5H_2O\}_\infty$ (NOTT-200-solv) and $\{Li_{1.5}(H_3O)_{0.5}[In_2(L^2)_2]\cdot 11H_2O\}_\infty$ (NOTT-201-solv) used the previously reported method.[40,41]

Preparation of NOTT-206-solv, $\{[(Hdma)(H_3O)][In_2(L^1)_2]\cdot 4DMF\cdot 5H_2O\}_\infty$. H_4L^1 (0.15 g, 0.29 mmol) and $In(NO_3)_3$ (0.089 g, 0.29 mmol) were mixed and dispersed in a mixture of DMF/CH_3CN (15 mL, 2:1 v/v). The resulting white slurry turned clear upon addition of 10 drops of 6 M HNO_3 solution. The solution was then heated to 90 °C for 1 day, and colorless octahedral crystals of NOTT-206 were separated by filtration, washed sequentially by DMF, and dried in air. Yield: 0.39 g (80%). The $Hdma^+$ cations are generated via decomposition of DMF. Elemental analysis (% calcd/found): $In_2O_{26}C_{74}H_{81}N_5$ (In 13.62/13.25; C 52.71/52.69; H 4.84/4.51; N 4.15/4.07). Selected IR

dx.doi.org/10.1021/ic200967b |*Inorg. Chem.* 2011, 50, 9374–9384

Table 1. Summary Data for the Crystal Structures

	NOTT-206-solv	NOTT-207-solv	NOTT-208-solv	NOTT-209-solv
formula	$C_{74}H_{81}In_2N_5O_{26}$	$C_{60}H_{62.4}In_2Li_{1.2}O_{30.8}$	$C_{42}H_{45}InN_3O_{12.5}$	$C_{80}H_{83.8}In_2Li_{1.4}O_{31.6}$
fwt	1686.08	1514.27	906.63	1790.23
T (K)	150(2)	100(2)	120(2)	150(2)
wavelength (Å)	0.6939/synchrotron	0.6889/synchrotron	0.6893/synchrotron	0.6889/synchrotron
space group	$P4_1$	$P2_1/n$	$C2/m$	$C2/m$
a (Å)	9.8480(2)	9.892(10)	45.040(5)	45.20(2)
b (Å)	9.8480(2)	9.617(9)	9.7592(10)	9.738(5)
c (Å)	35.059(1)	35.11(3)	9.9522(10)	9.944(3)
β (deg)	–	90.544(17)	102.486(2)	102.053(19)
V (Å^3)	3400.1(2)	3340(5)	4271.1(8)	4280(3)
Z	2	2	4	2
D_{calcd} (g/cm^3)	1.647	1.506	1.410	1.389
μ	0.771	0.778	0.619	0.620
$F(000)$	1732	1541	1868	1838
diffraction number total/unique	18 024/5073	10 536/3981	13 352/3257	9656/3388
R_{int}	0.039	0.038	0.040	0.038
R_1 [$F > 4\sigma(F)$] /wR_2 [all F^2]	0.040/0.097	0.111/0.268	0.077/0.219	0.085/0.200
GOF	1.06	1.01	1.03	0.97
difference map extrema (e Å^{-3})	−0.44−0.93	−1.65−3.76	−0.49−1.58	−1.06−1.05
CCDC number	799388	799389	799390	799391

(cm^{-1}): ν = 3620(m), 3009(m), 2956(w), 2801(w), 2326(w), 1720(s), 1435(m), 1360(vs), 1250(m), 1011(m), 918(m), 777(s), 663(w).

Preparation of NOTT-207-solv, $\{Li_{1.2}(H_3O)_{0.8}[In_2(L^1)_2]\cdot 14H_2O\}_\infty$. To prepare the Li$^+$-exchanged samples NOTT-207-solv, crystals of as-synthesized NOTT-206-solv were immersed in a saturated solution of LiCl in distilled water/acetone (1:1 v/v), respectively, at room temperature. The crystals were soaked for 10 days, and the LiCl solution was refreshed three times daily. Upon decanting the metal chloride solutions, the cation-exchanged crystals of NOTT-207-solv were rinsed and soaked in distilled water/acetone (1:1 v/v), respectively, for 3 days to remove residual free LiCl. Elemental analysis (% calcd/found): $In_2O_{30.8}C_{60}H_{62.4}Li_{1.2}$ (In 15.16/14.76; C 47.59/47.55; H 4.15/4.27; Li 0.55/0.53; N 0.0/0.0). Selected IR (cm^{-1}): ν = 3629(w), 3011(w), 2957(w), 2162(m), 1705(m), 1617(s), 1566(s), 1383 (vs), 1077(m), 916(m), 774(s), 656(w).

Preparation of NOTT-208-solv, $\{[H_2ppz][In_2(L^3)_2]\cdot 4DMF\cdot 5.5H_2O\}_\infty$. H_4L^3 (0.15 g, 0.27 mmol), piperazine (0.15 g, 1.8 mmol), and $In(NO_3)_3$ (0.081 g, 0.27 mmol) were mixed and dispersed in a mixture of DMF/CH_3CN (15 mL, 2:1 v/v). The resulting white slurry turned clear upon addition of 10 drops of 6 M HNO_3 solution. The solution was then heated to 90 °C for 1 day, and colorless octahedral crystals of NOTT-206 were separated by filtration and washed sequentially by DMF, and dried in air. Yield: 0.22 g (90%). Elemental analysis (% calcd/found): $In_2O_{25.5}C_{84}H_{87}N_6$ (In 12.63/12.26; C 55.49/55.53; H 4.82/5.03; N 4.62/4.76). Selected IR (cm^{-1}): ν = 3622(m), 3016 (m), 2950(w), 2800(w), 2336 (w), 1727(s), 1440(m), 1360(vs), 1252(m), 1011(m), 912(m), 770(s), 668(w).

Preparation of NOTT-209-solv, $\{Li_{1.4}(H_3O)_{0.6}[In_2(L^3)_2]\cdot 4acetone\cdot 11H_2O\}_\infty$. To prepare the Li$^+$-exchanged samples NOTT-209-solv, crystals of as-synthesized NOTT-208-solv were immersed in a saturated solution of LiCl in distilled water/acetone (1:1 v/v), respectively, at room temperature. The crystals were soaked for 10 days, and the LiCl solution was refreshed three times daily. Upon decanting the metal chloride solutions, the cation-exchanged crystals of NOTT-209-solv were rinsed and soaked in distilled water/acetone (1:1 v/v), respectively, for 3 days to remove residual free LiCl. Elemental analysis (% calcd/found): $In_2O_{31.6}C_{80}H_{83.8}Li_{1.4}$ (In 12.83/12.55; C 53.67/53.86; H 4.72/4.73; Li 0.54/0.52; N 0.0/0.0). Selected IR (cm^{-1}): ν = 3634(w), 3010(w), 2967(w), 2152(m), 1700(m), 1610(s), 1552(s), 1380 (vs), 1070(m), 926(m), 775(s), 656(w).

Single Crystal X-ray Diffraction Studies. X-ray diffraction data of single crystals of NOTT-206-solv and NOTT-208-solv were collected on Station 9.8 of the Synchrotron Radiation Source at STFC Daresbury Laboratory. X-ray diffraction data of single crystals of NOTT-207-solv and NOTT-209-solv were collected on Beamline I19 of the Diamond Light Source. The structures were solved by direct methods and developed by difference Fourier techniques using the SHELXTL software package (Table 1).[42] The hydrogen atoms on the ligands were placed geometrically and refined using a riding model. Geometric restraints were applied to the phenyl ring and the carboxylate group of the organic ligand. The unit cell volume includes a large region of disordered solvents which could not be modeled as discrete atomic sites. We employed PLATON/SQUEEZE[43,44] to calculate the contribution to the diffraction from the solvent region and thereby produced a set of solvent-free diffraction intensities. The final formula was calculated from the SQUEEZE results combined with elemental analysis and TGA data: the contents of the solvent/cation region are therefore represented in the unit cell contents but were not included in the refinement model.

Nitrogen and Hydrogen Isotherms. N_2 and H_2 adsorption isotherms were recorded at the University of Nottingham on an IGA system with a high resolution pressure transducer (Hiden Isochema, Warrington, U.K.) under ultrahigh vacuum in a clean system with a diaphragm and turbo pumping system. Samples were loaded into the IGA system and degassed at 120 °C, 10^{-10} bar for 24 h to give desolvated samples. In a typical procedure, ~100 mg of dry sample was used. Ultrapure plus grade (99.9995%) H_2 and ultrapure research grade (99.9999%) N_2 were purchased from BOC and purified further using calcium aluminosilicate and activated carbon adsorbents to remove trace amounts of water and other impurities before introduction into the IGA system. The density of bulk H_2 at 77 K in the buoyancy correction was calculated by the Redlich−Kwong−Soave equation of state of H_2 incorporated in the IGASWIN software of the IGA system. The density

dx.doi.org/10.1021/ic200967b |Inorg. Chem. 2011, 50, 9374–9384

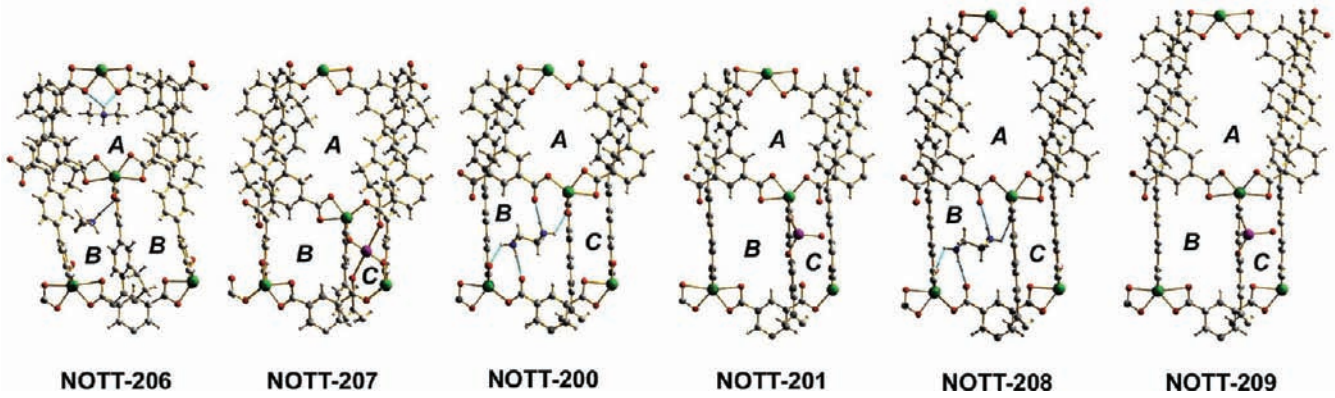

Figure 1. Views of the single crystal X-ray structures of the NOTT-MOF hosts studied herein (pores labeled as ***A***, ***B***, and ***C***). (Indium, green; oxygen, red; carbon, gray; hydrogen, white; nitrogen, blue; lithium, purple. The O···H−N hydrogen bonds are highlighted in cyan.)

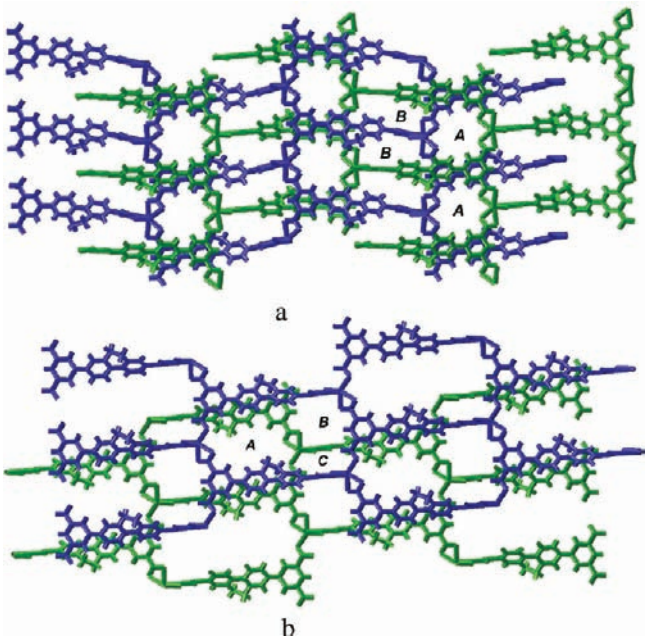

Figure 2. (a) View along the *b*-axis of the 2-fold interpenetrated structure of NOTT-206 containing two channels (labeled ***A*** and ***B***). (b) View along the *b*-axis of the 2-fold interpenetrated structure of NOTT-207 containing three channels (labeled ***A***, ***B***, and ***C***). The two independent networks are shown in blue and green. The cations in channels ***A*** and ***B*** of NOTT-206 or in channel ***C*** of NOTT-207 connect two independent networks into one single network via hydrogen bonding.

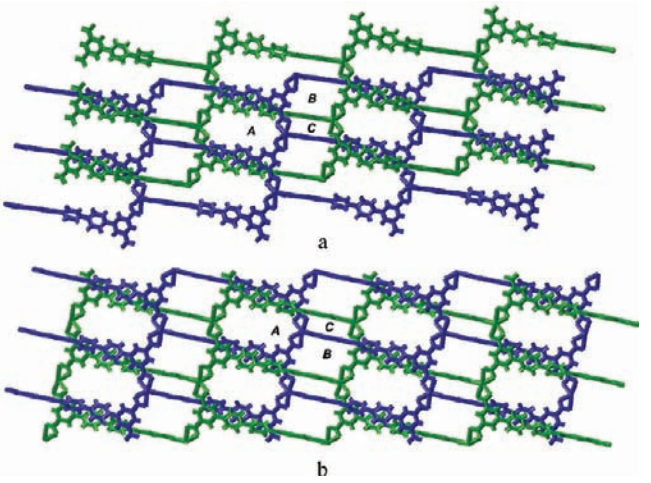

Figure 3. View along the *b*-axis of the 2-fold interpenetrated structure of (a) NOTT-208 and (b) NOTT-209 containing three channels (labeled ***A***, ***B***, and ***C***). The two independent networks are shown in blue and green. The cations in channel ***B*** of NOTT-208 or channel ***C*** of NOTT-209 connect two independent networks into one single network via hydrogen bonding.

of liquid H_2 at the boiling point (0.0708 g cm^{-3}) was used for the adsorbate buoyancy correction.

^{7}Li Solid-State NMR Measurements. Wideline ^{7}Li NMR spectra were recorded on a Varian InfinityPlus spectrometer operating at a Larmor frequency of 116.62 MHz. Powdered samples were sealed into 5 mm diameter glass tubes for measurements in a single-resonance solenoid coil probe at 298 K. A solid-echo pulse sequence was used with $\pi/2$ pulses of between 1.25 μs and an echo delay of 8.0 μs. Chemical shifts were referenced externally to 1.0 M LiCl (aq).

RESULTS AND DISCUSSION

Single Crystal X-ray Structures. Single crystal X-ray structural analyses confirm (Figure 1) the formation of three-dimensional 4-c coordination frameworks constructed from mononuclear $[In(O_2CR)_4]$ nodes bridged by tetracarboxylate ligands. Each In(III) center in NOTT-206-solv is 8-coordinate, and in NOTT-200-solv and NOTT-208-solv 7-fold coordination at In(III) is observed via binding to O-centers from four carboxylate groups to form in each case a tetrahedral 4-c node. Each deprotonated ligand binds to four In(III) centers and thus acts as a tetrahedral 4-c node to give an overall uninodal diamondoid class IIa ***dia*** topology.[45,46] The structures of NOTT-200-solv, NOTT-206-solv, and NOTT-208-solv are all doubly interpenetrated (Figures 2 and 3), and an alternative view based upon chemically different In(III) and ligand nodes can be considered. If the organic ligand is viewed as a rod with two 3-c nodes at its ends, the topology of this series of indium−carboxylate frameworks can be assigned as the very rare ***tfa*** (2-fold interpenetrated of class IIa) with point symbol $\{8^3\}_2\{8^6\}$ based upon binodal $(3\text{-c})_2(4\text{-c})$ nets (Figure 4).[47]

Three distinct interlinked channels, ***A***, ***B***, and ***C***, are formed in NOTT-200-solv and NOTT-208-solv by alternate overlapping of two independent networks. Channel ***A*** is occupied by free DMF and H_2O solvent molecules, while channel ***B*** contains only

dx.doi.org/10.1021/ic200967b |*Inorg. Chem.* 2011, 50, 9374–9384

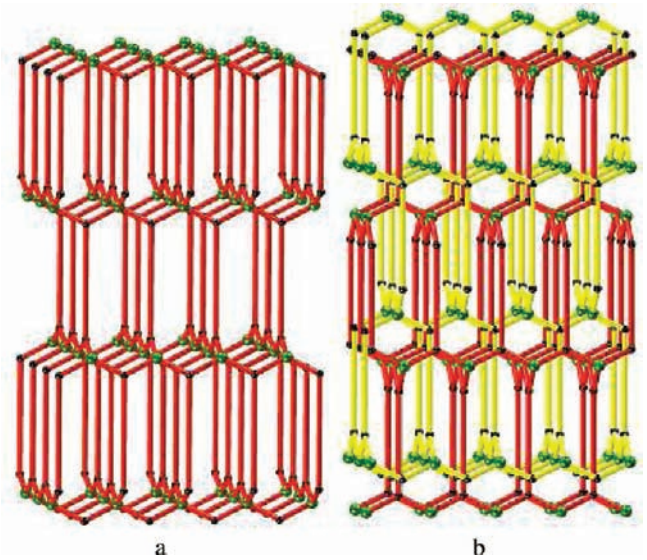

Figure 4. Views of the *tfa* network topology for (a) a single net and for (b) 2-fold interpenetrated nets. (Indium node, green; ligand node, black. Two independent nets are shown in red and yellow.)

ordered H_2ppz^{2+} dications. Channel ***C*** is empty because it is too narrow to allow the entrance of solvent molecules. The approximate dimensions of the channels, taking into account the van der Waals radii of the surface atoms, are 10.6 Å × 4.4 Å (channel ***A***), 4.3 Å × 4.1 Å (channel ***B***), and 4.6 Å × 1.0 Å (channel ***C***), with channels ***B*** and ***C*** interconnected along the *c*-axis. The sizes of channels ***B*** and ***C*** in NOTT-208-solv are the same as in NOTT-200-solv, while channel ***A*** is elongated by the increased length of the organic linker in NOTT-208-solv. N−H···O hydrogen bonding between two uncoordinated carboxylate oxygen centers located at the corners of channel ***B*** and the NH_2^+ groups of the H_2ppz^{2+} dications is observed. Thus, the size of channels ***B*** and ***C*** is defined by the H_2ppz^{2+} dications (Figure 1).

On Li^+-exchange, NOTT-208-solv undergoes a single-crystal-to-single-crystal transformation to NOTT-209-solv: the H_2ppz^{2+} dications that block channel ***B*** in NOTT-208-solv are replaced by Li^+ ions in channel ***C*** during the transformation, thus releasing the porosity of channel ***B*** in NOTT-209-solv. The Li^+ ion in NOTT-209-solv is tetrahedrally coordinated to four oxygen atoms: two from symmetry-related carboxylate groups, Li−O = 2.14(6) Å, and two from the coordinated water molecules, Li−O = 1.75(6), 1.98(5) Å (Figures 1 and 6). Comparison of the PXRD patterns for NOTT-208-solv with those for NOTT-209-solv shows near-identical patterns for these two frameworks, confirming retention of framework structure and absence of phase changes on Li^+-exchange (Figure 7). A similar single-crystal-to-single-crystal transformation is observed on going from NOTT-200-solv to NOTT-201-solv.

Replacement of the biphenyl group in the organic backbone of NOTT-200-solv with 9,10-dihydrophenanthrene affords NOTT-206-solv. This material crystallizes in a crystal system of higher symmetry (tetragonal, space group $P4_1$) with ordered orientation of the 9,10-dihydrophenanthrene groups pointing into the pore centers to form chiral channels parallel to the 4_1 screw axis along the crystallographic *c*-axis. The triporous unit observed in NOTT-200-solv has been simplified to a biporous structure in NOTT-206-solv, with only two types of interlinked channels, namely ***A*** (4.8 Å × 3.8 Å) and ***B*** (6.6 Å × 1.8 Å) (Figure 1). The $Hdma^+$ cations

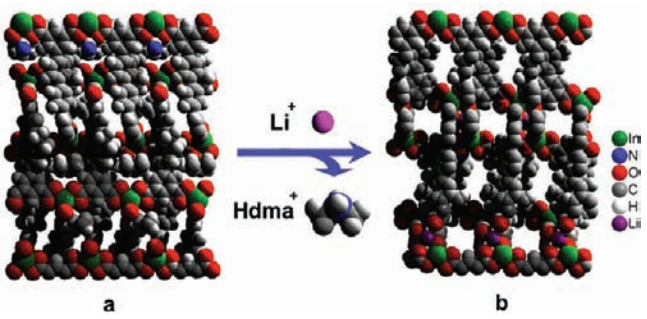

Figure 5. Space-filling views of the framework structures of (a) NOTT-206 and (b) NOTT-207 containing different cations within channels.

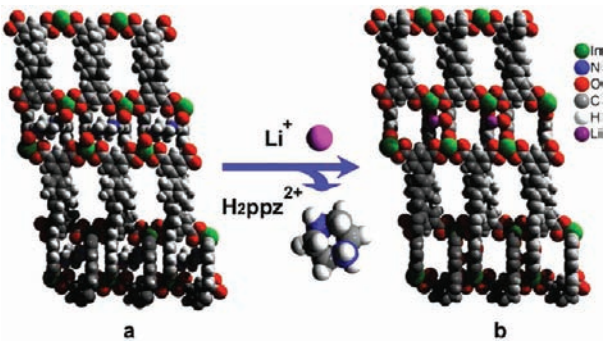

Figure 6. Space-filling views of the framework structures of (a) NOTT-208 and (b) NOTT-209 containing different cations within channels.

in NOTT-206-solv form N−H···O hydrogen bonds to the carboxylate oxygen atoms, and are located in both channel ***A*** and channel ***B***, but in different orientations to match the pore geometry. Thus, both channels in NOTT-206-solv are blocked with bulky $Hdma^+$ cations.

In contrast to NOTT-200-solv and NOTT-208-solv, upon Li^+-exchange NOTT-206-solv displays a single-crystal-to-single-crystal transformation with a phase transition from a tetragonal to a monoclinic system. Accordingly, the biporous channels ***A*** and ***B*** in NOTT-206-solv rearrange to give a triporous array composed of channels ***A***, ***B***, and ***C*** in NOTT-207-solv. The two independent networks in NOTT-206-solv shift toward each other during the Li^+-exchange, and the associated phase transition leads to a different size distribution of pores: 8.0 Å × 3.6 Å for channel ***A***, 3.8 Å × 4.0 Å for channel ***B***, and 2.4 Å × 1.0 Å for channel ***C***. Interestingly and importantly, the Li^+ ion in NOTT-207-solv is not bound to water molecules but is octahedrally coordinated by six oxygen atoms from six different carboxylate groups with Li−O bond lengths ranging from 2.007(15) to 2.464(16) Å. Such a coordination environment for Li^+ is distinct and rarely observed in coordination polymers.[48] The carboxylate oxygen atom O1 in channel ***C***, which was previously coordinated to the In(III) center at 2.285(6) Å in NOTT-206-solv, is now located much further from the In(III) center at 2.793 Å in NOTT-207-solv to form a 7-coordinate In(III) center in the latter framework. To balance this, two O1 atoms from each of the interpenetrated frameworks now protrude into channel ***C*** and anchor the Li^+ ions. Thus, Li^+ exchange to give NOTT-207-solv results in a diminished size for channel ***C*** while channel ***A*** has expanded (Figures 1 and 5). The phase change on going from NOTT-206-solv to NOTT-207-solv is confirmed by PXRD, which shows shifts in peak positions and changes in peak intensities (Figure 7).

dx.doi.org/10.1021/ic200967b |*Inorg. Chem.* 2011, 50, 9374–9384

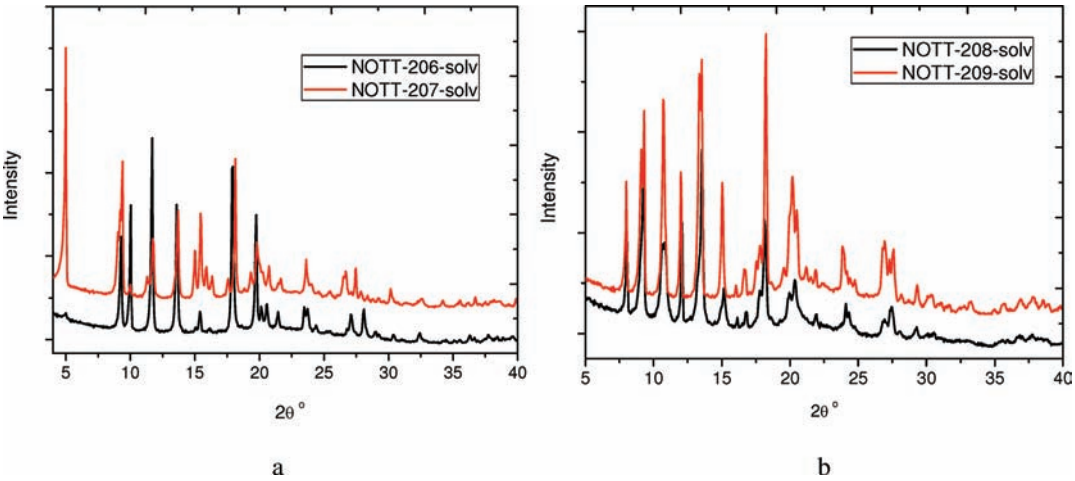

Figure 7. Comparison of PXRD patterns for (a) NOTT-206-solv and NOTT-207-solv and (b) NOTT-208-solv and NOTT-209-solv.

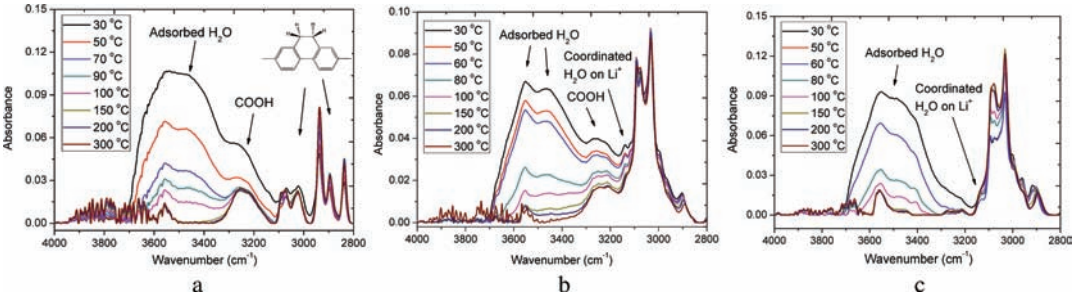

Figure 8. *In situ* IR spectra for (a) NOTT-207-solv, (b) NOTT-201a-solv, and (c) NOTT-209-solv under a flow of He.

Structural Thermal Stability. All framework complexes are stable after removal of solvent and coordinated water. All frameworks showed similar behavior by TGA with rapid loss of solvent under N_2 below 120 °C and stability up to 400 °C, above which the materials start to decompose. PXRD indicates that the solvent-free frameworks retain their original structure and unit cell (see Supporting Information).

***In Situ* IR Spectroscopy.** *In situ* IR spectroscopy of NOTT-201-solv and NOTT-209-solv confirms that the water molecules bound to Li^+ can be removed by heating at 100−150 °C under a flow of He gas. In fully dehydrated NOTT-201a and NOTT-209a, no combination of carboxylate groups is able to fully saturate the coordination sphere around the desolvated Li^+ cation, thus leaving the Li^+ center at least partially exposed. This is consistent with TGA results which indicate no further weight loss between 120 and 400 °C. In contrast, *in situ* IR spectroscopy of NOTT-207-solv confirms the absence of water molecules coordinated to the Li^+, consistent with the X-ray crystal structure, and adsorbed water molecules within the channels are removed rapidly with increasing temperature (Figure 8).

^{7}Li Solid-State NMR. Wideline ^{7}Li ($I = {}^3/_2$) NMR spectra (Figure 9) were recorded for powdered materials in order to characterize the structural changes which occur on desolvation. For a spin $^3/_2$ nucleus in a powdered sample the interaction between the nuclear quadrupole moment and the electric field gradient due to the surrounding bonds results in a narrow "central transition" line and two powder-broadened "satellite transition" lines. The frequency separation of the intensity maxima of the two satellites is related to the quadrupolar coupling constant C_Q which is a measure of the asymmetry of the local electronic environment. In NOTT-207-solv the Li^+ ion is octahedrally coordinated by six carboxylate oxygen atoms: the high symmetry of this environment leads to such a small value for C_Q that the satellites are not resolved from the central transition line. In NOTT-201-solv and NOTT-209-solv the Li^+ ion is tetrahedrally coordinated by two carboxylate oxygen atoms and two water molecules. This less symmetrical environment produces quadrupolar coupling constants of 50 ± 2 and 47 ± 2 kHz, which are large enough to be measured directly from the satellite separation. The ^{7}Li chemical shifts lie in the range −3.4 to −3.6 ppm, within the range expected for Li^+ bonded to oxygen. On desolvation, the spectrum of NOTT-207a is essentially unchanged, suggesting that the octahedral coordination of the Li^+ ion by carboxylate groups is retained. However, the spectra for both NOTT-201a and NOTT-209a show significant changes on desolvation with the value of C_Q increasing to 145 ± 2 kHz for both materials. This increase suggests a significant decrease in symmetry, consistent with the loss of the coordinated water molecules to give an asymmetric and open Li^+ center. This work represents the first example of the use of ^{7}Li solid-state NMR to monitor the structural and coordinative changes at Li^+ on desolvation in porous extended framework materials.

Nitrogen Isotherms. The acetone-exchanged samples NOTT-206-acetone, NOTT-207-acetone, NOTT-200-acetone, NOTT-201-acetone, NOTT-208-acetone, and NOTT-209-acetone are stable, but on heating to 100 °C at 10^{-10} bar for 24 h give the fully desolvated samples NOTT-206a, NOTT-207a, NOTT-200a, NOTT-201a, NOTT-208a, and NOTT-209a,

dx.doi.org/10.1021/ic200967b |*Inorg. Chem.* 2011, 50, 9374–9384

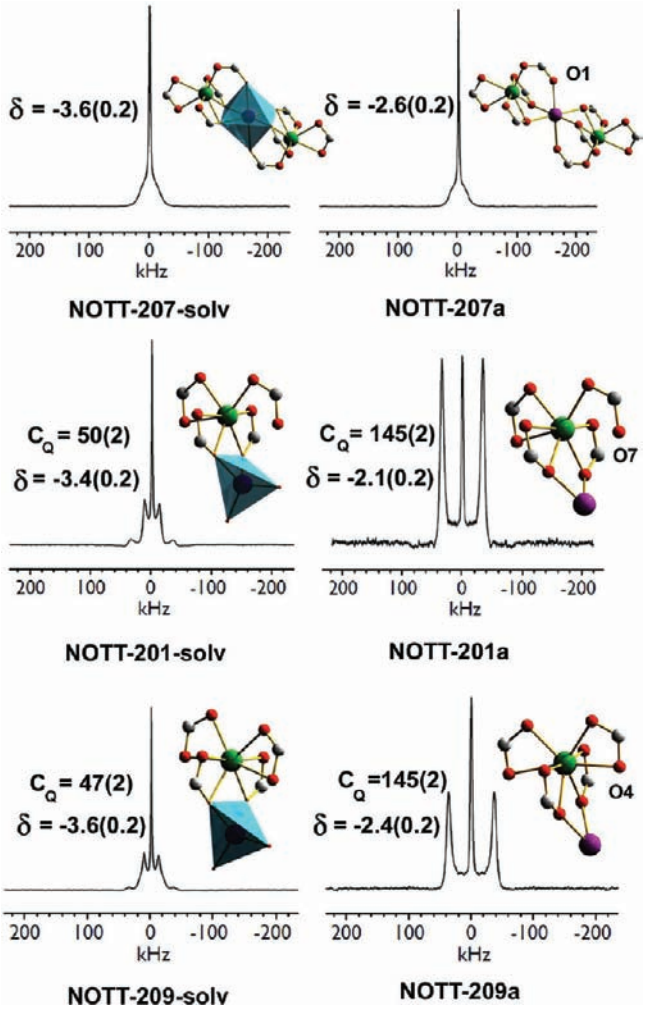

Figure 9. ^{7}Li solid-state NMR spectra and Li^{+} ion coordination environments in NOTT-207-solv, NOTT-207a, NOTT-201-solv, NOTT-201a, NOTT-209-solv, and NOTT-209a. The origin of the kHz scale corresponds to 0 ppm referenced externally to 1.0 M LiCl solution; a shift of 10 ppm corresponds to 1.166 kHz. The chemical shift δ is quoted in ppm, and quadrupolar coupling constant C_Q is in kHz. ^{7}Li satellite lines are not resolved from the central transition in NOTT-207-solv and NOTT-207a, and therefore, it is not possible to estimate the C_Q values in this case. (Indium, green; oxygen, red; carbon, gray; hydrogen, white; nitrogen, blue; lithium, purple. Coordination environments at Li^{+} in NOTT-207-solv, NOTT-201-solv, and NOTT-209-solv are shown as polyhedra.)

respectively. NOTT-206a does not show any apparent N_2 uptake at 77 K (Figure 10), because both pore channels ***A*** and ***B*** are blocked by $Hdma^{+}$ cations and by the 9,10-dihydrophenanthrene group in the backbone of the framework. However, the accessible internal BET surface area, estimated from the single crystal X-ray structure using a Monte Carlo integration where the probe N_2 molecule is rolled over the internal framework surface,[49] is calculated to be 138 $m^2\ g^{-1}$ for NOTT-206a. A PLATON/SQUEEZE[43,44] calculation using the single crystal structure data estimated that approximately 24% of the voids (corresponding to 0.191 $cm^3\ g^{-1}$ total micropore volume) are accessible indicating that although NOTT-206a is potentially porous, the pore entrances are blocked by the $Hdma^{+}$ cations (Table 2). By replacing the $Hdma^{+}$ cations with Li^{+} ions, channels ***A*** and ***B*** are both released, and adsorption of N_2 in NOTT-207a shows a typical type-I isotherm with little hysteresis, with a BET surface area of 474 $m^2\ g^{-1}$, entirely consistent with the Monte Carlo value of 475 $m^2\ g^{-1}$ calculated from the crystal structure (Table 2). Thus, by incorporating a Li^{+} ion in NOTT-207a, the internal surface area becomes fully available for N_2 uptake and release, confirming that the choice of pore gate can have a crucial effect on the nature of the internal porosity and on its selectivity.[50] Recently, Cooper et al. have reported organic solids in which porosity can be switched "on" or "off" in response to solid-state structural phase transitions linked to solvation and desolvation processes.[51] In contrast, in this study the framework porosity (in NOTT-206a and NOTT-207a) is switched "on" and "off" via cation exchange, representing a distinct route to modulate the porosity and gas uptake in porous solids.

Incorporating a combination of H_2ppz^{2+} dications and biphenyl tetracarboxylate, NOTT-200a shows a marked hysteresis loop for the N_2 adsorption and desorption isotherms at 77 K, while replacing the H_2ppz^{2+} dications with Li^{+} ions to give NOTT-201a leads to a typical type-I adsorption behavior with full reversibility and no hysteresis. The BET surface areas calculated for NOTT-200a and NOTT-201a are 180 and 580 $m^2\ g^{-1}$, respectively, confirming that the adsorption capacity of NOTT-201a is some 220% greater than that of NOTT-200a. Thus, the adsorption/desorption hysteresis and uptake capacities can be regulated and modulated by choosing the appropriate cation as the pore gate.

With the longer organic linker, both NOTT-208a and NOTT-209a display reversible type-I N_2 isotherms at 77 K without hysteresis (Figure 10), regardless of whether H_2ppz^{2+} or Li^{+} cations are in the channel. The BET surface areas calculated from the N_2 isotherm were found to be 687 and 729 $m^2\ g^{-1}$ for NOTT-208a and NOTT-209a, respectively, and are slightly smaller than the predicted Monte Carlo values of 852 and 902 $m^2\ g^{-1}$ for NOTT-208a and NOTT-209a, respectively (Table 2). These discrepancies can be attributed to the quality of the powder sample, and the inherent limitations of the BET theory.[49] Thus, incomplete solvent removal, partial framework collapse, and/or different pressure ranges employed for BET analysis could also be responsible for these discrepancies. The total microporous volume for NOTT-208a and NOTT-209a is estimated by maximum N_2 uptake at $P/P_0 = 1.0$ to be 0.287 and 0.303 $cm^3\ g^{-1}$, respectively. The pore size distribution is slightly wider for NOTT-209a than for NOTT-208a with the bulky dications in channel ***B*** in NOTT-208-solv replaced with smaller cations in channel ***C*** in NOTT-209-solv. Thus, with a longer organic linker H_4L^3, both NOTT-208a and NOTT-209a show similar BET surface area and microporous pore volume, despite incorporating different counter cations. This is distinct from the observations for NOTT-206a/NOTT-207a and NOTT-200a/NOTT-201a, indicating the pore environment/porosity in these charged materials are not solely controlled by cationic pore gates, but can be tuned by the choice of organic linkers.

Hydrogen Adsorption. Although N_2 molecules have restricted entry into NOTT-206a, the smaller kinetic diameter of H_2 means that NOTT-206a shows H_2 adsorption at 77 K, consistent with Monte Carlo BET surface area and accessible void calculations. NOTT-206a displays a stronger kinetic trap than NOTT-200a due to the 9,10-dihydrophenanthrene group combining with the bulky $Hdma^{+}$ cations to act as a reversible gate modulating the access of H_2 in and out of channels ***A*** and ***B***. NOTT-206a shows barely any desorption of H_2 from the

dx.doi.org/10.1021/ic200967b |*Inorg. Chem.* 2011, 50, 9374–9384

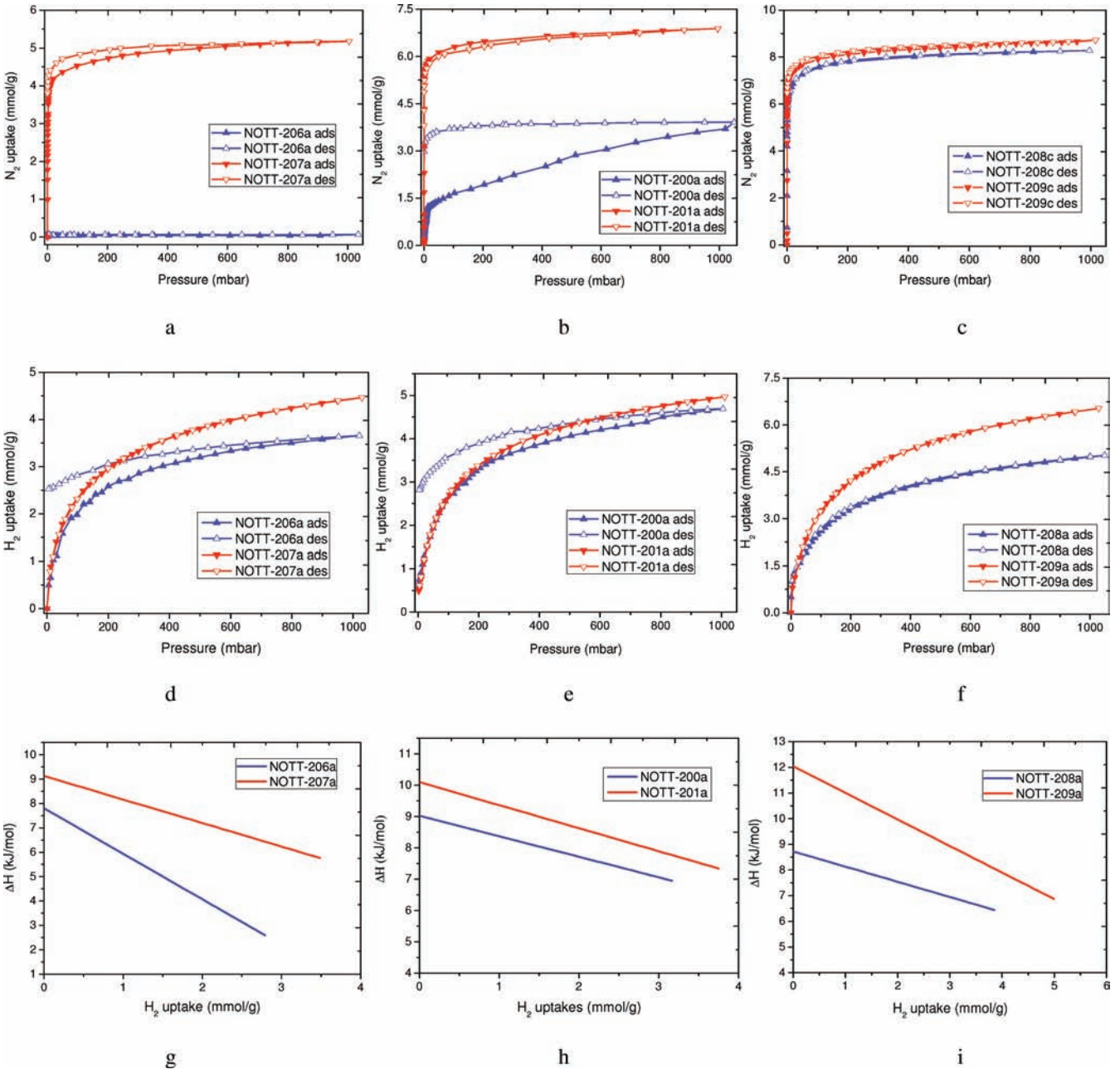

Figure 10. Gas adsorption isotherms and analyses for NOTT-206a, NOTT-207a, NOTT-200a, NOTT-201a, NOTT-208a, and NOTT-209a: (a−c) N_2 sorption isotherms at 77 K; (d−f) H_2 sorption isotherms at 77 K; (g−i) analyses of isosteric heats of adsorption for H_2.

framework on reducing pressure from 1.0 to 0.5 bar, and 70% of the adsorbed H_2 remains trapped down to 0.005 bar (Figure 10). In contrast, the H_2 isotherms for NOTT-207a show full reversibility with no hysteresis. Although the N_2 isotherms show dramatically different storage capacities between NOTT-206a and NOTT-207a, the H_2 uptake capacities at 77 K differ by only 22%. This most likely originates from the different kinetic diameters of H_2 (2.89 Å) and N_2 (3.64 Å), and the presence of voids within these materials which are large enough to accommodate H_2 but too small for N_2.

Both NOTT-208a and NOTT-209a show reversible H_2 sorption isotherms without hysteresis, consistent with their larger pores. The total H_2 uptakes at 1.0 bar for NOTT-208a and NOTT-209a are 4.97 and 6.53 mmol g^{-1}, respectively. Thus, there is an enhancement of 31% in H_2 storage capacity on going from NOTT-208a to NOTT-209a (Figure 10), much larger than for NOTT-206a/NOTT-207a (22%) and NOTT-200a/NOTT-201a (6.0%) under the same conditions. Interestingly, NOTT-208a and NOTT-209a show only small apparent differences in their N_2 uptake capacity (micropore volume) or BET surface area (Table 2), compared with other complexes in this series. Furthermore, given that NOTT-208a and NOTT-209a have identical framework structures, the enhancement in H_2 storage capacities can be linked to the cations, H_2ppz^{2+} or Li^+, residing in the channels.

Using a density of 0.0708 g cm^{-3} for H_2 at its boiling point of 20.28 K, it can be deduced that the volumes of H_2 adsorbed in NOTT-206a and NOTT-207a at 1.0 bar correspond to 55% and

dx.doi.org/10.1021/ic200967b |*Inorg. Chem.* 2011, 50, 9374–9384

Table 2. Physical Parameters for Charged Metal−Organic Framework Materials in This Study

	NOTT-206a	NOTT-207a	NOTT-200a	NOTT-201a	NOTT-208a	NOTT-209a
formula (activated)	$[Hdma]H[In_2(L^1)_2]$	$Li_{1.2}H_{0.8}[In_2(L^1)_2]$	$[H_2ppz][In_2(L^2)_2]$	$Li_{1.5}H_{0.5}[In_2(L^2)_2]$	$[H_2ppz][In_2(L^3)_2]$	$Li_{1.4}H_{0.6}[In_2(L^3)_2]$
channel ***A*** size (Å)	4.8 × 3.8	8.0 × 3.6	6.6 × 4.4	6.1 × 4.4	10.6 × 4.4	10.1 × 4.4
channel ***B*** size (Å)	6.6 × 1.8	3.8 × 4.0	4.3 × 4.1	4.9 × 4.1	4.3 × 4.1	5.0 × 4.1
channel ***C*** size (Å)	n.a.	2.4 × 1.0	4.6 × 1.0	4.5 × 1.0	4.6 × 1.0	4.6 × 1.0
cations/pore gate	$Hdma^+$	Li^+	H_2ppz^{2+}	Li^+	H_2ppz^{2+}	Li^+
channel with gate	***A, B***	***C***	***B***	***C***	***B***	***C***
maximum N_2 uptake (mmol/g)	∼0	5.18	3.92	6.88	8.28	8.73
BET surface area[a] (m^2/g)	∼3	474	180	580	687	729
BET surface area[b] (m^2/g)	138	475	373	643	852	902
evacuated framework density (g/cm^3)	1.256	1.241	1.212	1.165	1.110	1.047
accessible void[c] (%)	24	40	35	42	39	43
pore volume[a] (N_2) (cm^3/g)	∼0	0.206	0.136	0.239	0.287	0.303
pore volume[c] (cm^3/g)	0.191	0.322	0.289	0.360	0.351	0.410
pore size (N_2) (Å)	∼0	7.4	4.3	8.3	6.9	7.2
H_2 uptake (1/20 bar) (mmol/g)	3.66/5.43	4.46/6.51	4.69/6.64	4.97/9.38	4.97/8.75	6.53/10.57
H_2 filling ratio[d] (1/20 bar) (%)	55/81	39/58	47/67	40/76	40/71	45/74
adsorption enthalpy[e] (kJ/mol)	7.81	9.13	9.03	10.10	8.73	12.04

[a] From N_2 isotherm at 77 K. [b] From Monte Carlo simulation. [c] From PLATON/SOLV[43] with probe size of 1.2 Å. [d] With total pore volume from N_2 isotherm at 77 K. [e] At zero surface coverage.

39% filling of the total crystallographically determined extra-framework/cation pore volumes of 0.191 and 0.322 $cm^3\ g^{-1}$ for NOTT-206a and NOTT-207a, respectively. At 20 bar up to 81% and 58% of the total pore volume can be filled by H_2 molecules in NOTT-206a and NOTT-207a, respectively. These values are reasonable considering that the adsorption temperature is well above the H_2 critical temperature (33 K) and are similar to those observed for NOTT-200a and NOTT-201a (Table 2). It is also reasonable to expect increased H_2 uptake for NOTT-207a in comparison to NOTT-206a due to the increase in the available pore volume and BET surface area in the host material. In contrast, for NOTT-208a and NOTT-209a, the adsorbed H_2 filling ratios at 77 K are 40% and 45%, respectively, at 1.0 bar, and increase to 71% and 74% at 20 bar. H_2 molecules pack more efficiently in NOTT-209a across the pressure range since this host has Li^+ cations acting as a pore gate, leading to significant enhancement in H_2 uptake capacity.

Isosteric Heat of Hydrogen Adsorption. The isosteric heat of adsorption Q_{st} was determined by fitting a virial-type equation to the H_2 adsorption isotherms at 77 and 87 K. The $ln(p)$ values for a given amount adsorbed (n) were calculated from the linear regressions determined from the virial equation analysis using the following virial equation.[52,53]

$$\ln(n/p) = A_0 + A_1 n + A_2 n^2 \ldots \quad (1)$$

Here, p is pressure, n is amount adsorbed, and A_0, A_1, etc. are virial coefficients.

Virial analysis of the H_2 adsorption isotherms measured at 77 and 87 K revealed that the isosteric heat of adsorption at zero surface coverage is 7.8 and 9.1 kJ mol^{-1} for NOTT-206a and NOTT-207a, respectively. Given that the Li^+ ions have a complete octahedral coordination sphere in NOTT-207a and so are not directly accessible to the H_2 molecules, the enhancement of the H_2 adsorption enthalpy on going from NOTT-206a to NOTT-207a is attributed to the framework phase transition during the cation exchange, from tetragonal to monoclinic, with charge distributions being more heterogeneous on framework surface with the lower symmetry. Similar enhancements of ∼2 kJ mol^{-1} in the H_2 adsorption enthalpy have been observed by decreasing the pore surface symmetry through hydrogenation of the organic ligand.[54]

Using the same virial analysis, NOTT-208a and NOTT-209a give values of 8.7 and 12.0 kJ mol^{-1}, respectively, for the isosteric heat of adsorption for H_2 at zero surface coverage. With the same H_2ppz^{2+} cation and similar channel size, the adsorption enthalpy of NOTT-208a is comparable to that observed for NOTT-200a (9.0 kJ mol^{-1}). However, with the same framework structure and a pore surface chemistry defined by the carboxylate ligand and the In(III) building blocks, NOTT-209a shows a 38% increase in the initial heat of adsorption, and furthermore, it is ∼2−3 kJ mol^{-1} higher than NOTT-208a at all measured H_2 loadings. Significantly, the presence of the smaller Li^+ ion leads to an increase in both the uptake capacity and the heat of adsorption for H_2 storage in NOTT-209a compared to NOTT-208a, even though both desolvated materials give similar BET surface areas and micropore volumes. The uptake capacity and the heat of adsorption for H_2 storage materials are normally inversely related, especially in the MOF materials with large pore volumes/sizes.[16,20] This is physically reasonable, because it has been well established that smaller pores afford stronger overlapping potentials for H_2 molecules and thus higher heats of adsorption.[4,20] It is worth mentioning that simultaneous increase of these two parameters by post-synthetic modification has been reported previously[35,36,55,56] but only in narrow pore materials. However, the changes in the pore size upon post-synthetic modification in these latter systems have not been reported. In contrast, NOTT-209a in this study also shows simultaneous increase on pore size and heat of adsorption, two parameters that are also normally inversely related. Interestingly, Snurr et al. have very recently properties a computational study on H_2 storage properties in several doped MOFs.[57] They found that doped Li^+

dx.doi.org/10.1021/ic200967b |*Inorg. Chem.* 2011, 50, 9374–9384

Scheme 2. Modulation of Gas Adsorption Properties with Different "Pore Gates" in NOTT-MOF Materials[a]

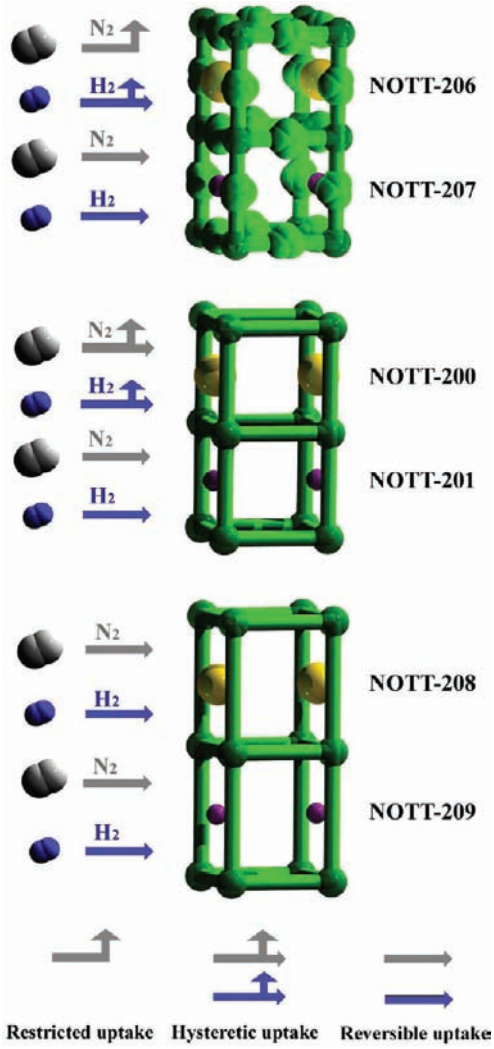

[a] The doubly-interpenetrated $(3\text{-c})_2(4\text{-c})$ ***tfa*** nets in these materials have been simplified to non-interpenetrated 6-c ***pcu*** cages for purposes of clarity.

ions bind H_2 too weakly (~ -10 kJmol^{-1}) to enhance overall adsorption capacity at ambient temperatures, even at 100 bar. In particular, Mg^{2+} ions have been suggested as promising alternatives to Li^+ ions to efficiently (~ -22 kJmol^{-1}) bind H_2 molecules, leading to the enhancement of H_2 storage at ambient temperatures.[57] Therefore, doping of the current series of anionic MOFs with Mg^{2+} and other cations ions might be an optimal way to further increase the heat of adsorption for H_2 storage at near ambient conditions.

CONCLUSIONS

The presence of cations, coupled with organic ligand functionality, affords a tunable pore environment and provides opportunities for uncovering novel gas separation/storage properties in MOF materials (Scheme 2). Amine-based organic cations can act as bulky gates to block channels, and provide opportunities to restrict, trap, or accommodate gas molecules. The smaller inorganic Li^+ cations can open up the channel and allow rapid gas uptake and release, with an increase in both capacity and heat of adsorption of H_2. Significantly, the structural and coordinative changes at Li^+ sites in this series of materials have been investigated by ^{7}Li solid-state NMR spectroscopy, providing important and direct evidence underpinning the observed enhanced H_2 storage properties on Li^+-doping. These findings demonstrate that the gas storage properties of charged MOFs are controllable by appropriate choice of counterions, supporting the postulate that the incorporation of different cations within pores may act as a code for the enhancement of H_2 storage properties and generating new materials properties.

ASSOCIATED CONTENT

Supporting Information. Crystallographic information files (CIFs), experimental details, additional views of the crystal structures, TGA, PXRD, technical details for gas adsorption experiments, and analysis of gas adsorption isotherms. This material is available free of charge via the Internet at http://pubs.acs.org.

AUTHOR INFORMATION

Corresponding Author

*E-mail: Neil.Champness@nottingham.ac.uk (N.R.C.); M.Schroder@nottingham.ac.uk (M.S.). Fax: +44 115 951 3563.

ACKNOWLEDGMENT

We thank EPSRC and the University of Nottingham for support. M.S. and N.R.C. gratefully acknowledge receipt of an ERC Advanced Grant and a Royal Society Leverhulme Trust Senior Research Fellowship, respectively. We thank STFC for access to Station 9.8 of the Daresbury Laboratory Synchrotron Radiation Source and to Beamline I19 of Diamond Light Source. We thank the EPSRC National Crystallography Service and Prof. W. Clegg, Dr. P.J. Rizkallah, Dr. S.A. Barnett, and Dr. H. Nowell for experimental assistance. We thank Dr. G. S. Walker for IR spectroscopy. S.Y. thanks Shell-EPSRC for a DHPA fellowship and EPSRC for a PhD Plus Fellowship.

REFERENCES

(1) Kaye, S. S.; Long, J. R. *J. Am. Chem. Soc.* **2005**, *127*, 6506–6507.
(2) Chapman, K. W.; Chupas, P. J.; Maxey, E. R.; Richardson, J. W. *Chem. Commun.* **2006**, 4013–4015.
(3) Dincă, M.; Dailly, A.; Liu, Y.; Brown, C. M.; Neumann, D. A.; Long, J. R. *J. Am. Chem. Soc.* **2006**, *128*, 16876–16883.
(4) Dincă, M.; Han, W. S.; Liu, Y.; Dailly, A.; Brown, C. M.; Long, J. R. *Angew. Chem., Int. Ed.* **2007**, *46*, 1419–1422.
(5) Dincă, M.; Long, J. R. *J. Am. Chem. Soc.* **2007**, *129*, 11172–11176.
(6) Nouar, F.; Eckert, J.; Eubank, J. F.; Forster, P.; Eddaoudi, M. *J. Am. Chem. Soc.* **2009**, *131*, 2864–2870.
(7) Chen, S.; Zhang, J.; Wu, T.; Feng, P.; Bu, X. *J. Am. Chem. Soc.* **2009**, *131*, 16027–16029.
(8) Liu, Y.; Eubank, J. F.; Cairns, A. J.; Eckert, J.; Kravtsov, V. C.; Luebke, R.; Eddaoudi, M. *Angew. Chem., Int. Ed.* **2007**, *46*, 3278–3283.
(9) Nouar, F.; Eubank, J. F.; Bousquet, T.; Wojtas, L.; Zaworotko, M. J.; Eddaoudi, M. *J. Am. Chem. Soc.* **2008**, *130*, 1833–1835.
(10) An, J.; Rosi, N. L. *J. Am. Chem. Soc.* **2010**, *132*, 5578–5579.
(11) Sava, D. F.; Kravtsov, V. C.; Nouar, F.; Wojtas, L.; Eubank, J. F.; Eddaoudi, M. *J. Am. Chem. Soc.* **2008**, *130*, 3768–3770.
(12) Lin, X.; Jia, J.; Hubberstey, P.; Schröder, M.; Champness, N. R. *CrystEngComm* **2007**, *9*, 438–448.

(13) Lin, X.; Champness, N. R.; Schröder, M. *Top. Curr. Chem.* **2010**, *293*, 35–76.
(14) Farha, O. K.; Yazaydin, A. Ö.; Eryazici, I.; Malliakas, C. D.; Hauser, B. G.; Kanatzidis, M. G.; Nguyen, S. T.; Snurr, R. Q.; Hupp, J. T. *Nat. Chem.* **2010**, *2*, 944–948.
(15) Furukawa, H.; Ko, N.; Go, Y. B.; Aratani, N.; Choi, S. B.; Choi, E.; Yazaydin, A. ö.; Snurr, R. Q.; O'Keeffe, M.; Kim, J.; Yaghi, O. M. *Science* **2010**, *329*, 424–428.
(16) Yan, Y.; Telepeni, I.; Yang, S.; Lin, X.; Kockelmann, W.; Dailly, A.; Blake, A. J.; Lewis, W.; Walker, G. S.; Allan, D. R.; Barnett, S. A.; Champness, N. R.; Schröder, M. *J. Am. Chem. Soc.* **2010**, *132*, 4092–4094.
(17) Yan, Y.; Lin, X.; Yang, S.; Blake, A. J.; Dailly, A.; Champness, N. R.; Hubberstey, P.; Schröder, M. *Chem. Commun.* **2009**, 1025–1027.
(18) Yuan, D.; Zhao, D.; Sun, D.; Zhou, H. C. *Angew. Chem., Int. Ed.* **2010**, *49*, 5357–5361.
(19) Lin, X.; Jia, J.; Zhao, X.; Thomas, K. M.; Blake, A. J.; Walker, G. S.; Champness, N. R.; Hubberstey, P.; Schröder, M. *Angew. Chem., Int. Ed.* **2006**, *45*, 7358–7364.
(20) Lin, X.; Telepeni, I.; Blake, A. J.; Dailly, A.; Brown, C. M.; Simmons, J. M.; Zoppi, M.; Walker, G. S.; Thomas, K. M.; Mays, T. J.; Hubberstey, P.; Champness, N. R.; Schröder, M. *J. Am. Chem. Soc.* **2009**, *131*, 2159–2171.
(21) Blake, A. J.; Champness, N. R.; Chung, S. S. M.; Li, W. S.; Schröder, M. *Chem. Commun.* **1997**, 1005–1006.
(22) Blake, A. J.; Champness, N. R.; Khlobystov, A. N.; Lemenovskii, D. A.; Li, W. S.; Schröder, M. *Chem. Commun.* **1997**, 1339–1340.
(23) Lin, Z.; Jiang, F.; Chen, L.; Yue, C.; Yuan, D.; Lan, A.; Hong, M. *Cryst. Growth Des.* **2007**, *7*, 1712–1715.
(24) Patarin, J. *Angew. Chem., Int. Ed.* **2004**, *43*, 3878–3880.
(25) Davis, M. E. *Nature* **2002**, *417*, 813–821.
(26) Khlobystov, A. N.; Champness, N. R.; Roberts, C. J.; Tendler, S. J. B.; Thompson, C.; Schröder, M. *CrystEngComm* **2002**, *4*, 426–431.
(27) Cui, X.; Khlobystov, A. N.; Chen, X.; Marsh, D. H.; Blake, A. J.; Lewis, W.; Champness, N. R.; Roberts, C. J.; Schröder, M. *Chem.—Eur. J.* **2009**, *15*, 8861–8873. Thompson, C.; Allen, S.; Champness, N. R.; Davies, M. C.; Khlobystov, A. N.; Roberts, C. J.; Schröder, M.; Tendler, S. J. B.; Wilkinson, M. J.; Williams, P. M. *J. Microscopy* **2004**, *214*, 261–271.
(28) Blomqvist, A.; Araujo, C. M.; Srepusharawoot, P.; Ahuja, R. *Proc. Natl. Acad. Sci. U. S. A.* **2007**, *104*, 20173–20176.
(29) Han, S. S.; Goddard, W. A. *J. Phys. Chem. C* **2008**, *112*, 13431–13436.
(30) Klontzas, E.; Mavrandonakis, A.; Tylianakis, E.; Froudakis, G. E. *Nano Lett.* **2008**, *8*, 1572–1576.
(31) Mavrandonakis, A.; Tylianakis, E.; Stubos, A. K.; Froudakis, G. E. *J. Phys. Chem. C* **2008**, *112*, 7290–7294.
(32) Dalach, P.; Frost, H.; Snurr, R. Q.; Ellis, D. E. *J. Phys. Chem. C* **2008**, *112*, 9278–9284.
(33) Cao, D.; Lan, J.; Wang, W.; Smit, B. *Angew. Chem., Int. Ed.* **2009**, *48*, 4730–4733.
(34) Bae, Y. S.; Snurr, R. Q. *Microporous Mesoporous Mater.* **2010**, *132*, 300–303.
(35) Mulfort, K. L.; Hupp, J. T. *J. Am. Chem. Soc.* **2007**, *129*, 9604–9605.
(36) Mulfort, K. L.; Hupp, J. T. *Inorg. Chem.* **2008**, *47*, 7936–7938.
(37) Mulfort, K. L.; Wilson, T. M.; Wasielewski, M. R.; Hupp, J. T. *Langmuir* **2009**, *25*, 503–508.
(38) Liu, Y. L.; Kravtsov, V. C.; Eddaoudi, M. *Angew. Chem., Int. Ed.* **2008**, *47*, 8446–8449.
(39) Bhatia, S. K.; Myers, A. L. *Langmuir* **2006**, *22*, 1688–1700.
(40) Yang, S.; Lin, X.; Blake, A. J.; Thomas, K. M.; Hubberstey, P.; Champness, N. R.; Schröder, M. *Chem. Commun.* **2008**, 6108–6110.
(41) Yang, S.; Lin, X.; Blake, A. J.; Walker, G. S.; Hubberstey, P.; Champness, N. R.; Schröder, M. *Nat. Chem.* **2009**, *1*, 487–493.
(42) Sheldrick, G. M. *Acta Crystallogr., Sect. A* **2008**, *64*, 112–122.
(43) Spek, A. L. *Acta Crystallogr., Sect. D* **2009**, *65*, 148–155.
(44) van der Sluis, P.; Spek, A. L. *Acta Crystallogr., Sect. A* **1990**, *46*, 194–201.
(45) Alexandrov, E. V.; Blatov, V. A.; Kochetkov, A. V.; Proserpio, D. M. *CrystEngComm* **2011**, *13*, 3947–3958.
(46) Baburin, I. A.; Blatov, V. A.; Carlucci, L.; Ciani, G.; Proserpio, D. M. *Cryst. Growth Des.* **2008**, *8*, 519–539.
(47) Hawxwell, S. M.; Espallargas, G. M.; Bradshaw, D.; Rosseinsky, M. J.; Prior, T. J.; Florence, A. J.; van de Streek, J.; Brammer, L. *Chem. Commun.* **2007**, 1532–1534.
(48) Olsher, U.; Izatt, R. M.; Bradshaw, J. S.; Dalley, N. K. *Chem. Rev.* **1991**, *91*, 137–164.
(49) Düren, T.; Millange, F.; Férey, G.; Walton, K. S.; Snurr, R. Q. *J. Phys. Chem. C* **2007**, *111*, 15350–15356.
(50) Li, J.; Kuppler, R. J.; Zhou, H. C. *Chem. Soc. Rev.* **2009**, *38*, 1477–1504.
(51) Jones, J. T. A.; Holden, D.; Mitra, T.; Hasell, T.; Adams, D. J.; Jelfs, K. E.; Trewin, A.; Willock, D. J.; Day, G. M.; Bacsa, J.; Steiner, A.; Cooper, A. I. *Angew. Chem., Int. Ed.* **2011**, *50*, 749–753.
(52) Ravikovitch, P. I.; Wei, D.; Chueh, W. T.; Haller, G. L.; Neimark, A. V. *J. Phys. Chem. B* **1997**, *101*, 3671–3679.
(53) Chen, B.; Zhao, X.; Putkham, A.; Hong, K.; Lobkovsky, E. B.; Hurtado, E. J.; Fletcher, A. J.; Thomas, K. M. *J. Am. Chem. Soc.* **2008**, *130*, 6411–6423.
(54) Yang, S.; Lin, X.; Dailly, A.; Blake, A. J.; Hubberstey, P.; Champness, N. R.; Schröder, M. *Chem.—Eur. J.* **2009**, *15*, 4829–4835.
(55) Mulfort, K. L.; Farha, O. K.; Stern, C. L.; Sarjeant, A. A.; Hupp, J. T. *J. Am. Chem. Soc.* **2009**, *131*, 3866–3868.
(56) Himsl, D.; Wallacher, D.; Hartmann, M. *Angew. Chem., Int. Ed.* **2009**, *48*, 4639–4642.
(57) Getman, R. B.; Miller, J. H.; Wang, K.; Snurr, R. Q. *J. Phys. Chem. C* **2010**, *115*, 2066–2075.